Chemie der Erde 77 (2017) 169–181

Contents lists available at ScienceDirect

Chemie der Erde

journal homepage: www.elsevier.de/chemer

In–situ LA–ICP–MS trace elemental analyzes of magnetite: The Tieshan skarn Fe–Cu deposit, Eastern China

Minfang Wang[a,*], Wei Wang[a,b], Kun Liu[a], Przemysław P. Michalak[c], Ketao Wei[d], Mingyue Hu[e]

[a] *Faculty of Earth Resources, China University of Geosciences, Wuhan, Hubei, 430074, China*
[b] *Faculty of Education and Psychology, Guangxi Science & Technology Normal University, Laibin, Guangxi, 546100, China*
[c] *Institute of Mineralogy, Technische Universität Bergakademie Freiberg, 09596 Freiberg, Germany*
[d] *The First Geological Brigade of Hubei Geological Bureau, Daye, Hubei, 435100, China*
[e] *National Research Center of Geoanalysis, Chinese Academy of Geological Sciences, Beijing 100037, China*

ARTICLE INFO

Article history:
Received 27 April 2016
Received in revised form 14 October 2016
Accepted 10 November 2016
Editorial handling - Juraj Majzlan

Keywords:
Magnetite
Trace elemental composition
LA–ICP–MS
Tieshan Fe–Cu deposit
Eastern China

ABSTRACT

The Tieshan Fe–Cu deposit is located in the Edong district, which represents the westernmost and largest region within the Middle–Lower Yangtze River Metallogenic Belt (YRMB), Eastern China. Skarn Fe–Cu mineralization is spatially associated with the Tieshan pluton, which intruded carbonates of the Lower Triassic Daye Formation. Ore bodies are predominantly located along the contact between the diorite or quartz diorite and marbles/dolomitic marbles. This study investigates the mineral chemistry of magnetite in different skarn ore bodies. The contrasting composition of magnetite obtained are used to suggest different mechanisms of formation for magnetite in the western and eastern part of the Tieshan Fe–Cu deposit. A total of 178 grains of magnetite from four magnetite ore samples are analyzed by LA–ICP–MS, indicating a wide range of trace element contents, such as V (13.61–542.36 ppm), Cr (0.003–383.96 ppm), Co (11.12–187.55 ppm) and Ni (0.19–147.41 ppm), *etc.* The Ti/V ratio of magnetite from the Xiangbishan (western part of the Tieshan deposit) and Jianshan ore body (eastern part of the Tieshan deposit) ranges from 1.32 to 5.24, and 1.31 to 10.34, respectively, indicating a relatively reduced depositional environment in the Xiangbishan ore body. Incorporation of Ti and Al in magnetite are temperature dependent, which hence propose that the temperature of hydrothermal fluid from the Jianshan ore body (Al = 3747–9648 ppm, with 6381 ppm as an average; Ti = 381.7–952.0 ppm, with 628.2 ppm as an average) was higher than the Xiangbishan ore body (Al = 2011–11122 ppm, with 5997 ppm as an average, Ti = 302.5–734.8, with 530.8 ppm as an average), indicating a down–temperature precipitation trend from the Jianshan ore body to the Xiangbishan ore body. In addition, in the Ca + Al + Mn versus Ti + V diagram, magnetite is plotted in the skarn field, consideration with the ternary diagram of TiO_2–Al_2O_3–MgO, proposing that the magnetite ores are formed by replacement, instead of directly crystallized from iron oxide melts, which provide a better understanding regarding the composition of ore fluids and processes responsible for Fe mineralization in the Tieshan Fe–Cu deposit.

1. Introduction

Magnetite is a common oxide mineral in rocks and it is an important petrogenetic indicator and pathfinder mineral for its compositional variability in a wide variety of iron deposit types (Deer et al., 1992; Dupuis and Beaudoin, 2011; Nadoll et al., 2014). Multi–element studies of sulfides as well as of oxides are of particular concern for geologists, where also spatial information on element distribution is important (Nesbitt et al., 1997). Recent years, there have been particular interests in magnetite composition, especially trace elemental composition for the understanding of the origin of different mineralization styles (Carrew, 2004; Chen et al., 2015; Chung et al., 2015; Dare et al., 2012; Dupuis and Beaudoin, 2011; Hu et al., 2014; Huang et al., 2015, 2016; Knipping et al., 2015b; Müller et al., 2003; Nadoll et al., 2012, 2014, 2015; Nadoll and Koenig, 2011; Singoyi et al., 2006; Zhao and Zhou, 2015). Laser ablation inductively coupled plasma mass spectrometry (LA–ICP–MS) technique provides *in–situ* measurement of many trace element with detection limits as low as sub ppm (Dupuis and Beaudoin, 2011; Liu et al., 2008; Nadoll and Koenig, 2011),

* Corresponding author.
E-mail address: wang_minfang@163.com (M. Wang).

http://dx.doi.org/10.1016/j.chemer.2016.11.002
0009-2819/

which makes trace elemental composition of magnetite becomes readily accessible. The reason why magnetite could be petrogenetic indicator and pathfinder mineral is that its compositional variability is largely dependent on physicochemical parameters of the magnetite–forming system, including temperature, oxygen fugacity (fO_2), sulfur fugacity (fS_2), silica activity, and melt/fluid composition (Nadoll et al., 2012, and references therein).

The Tieshan Fe–Cu deposit is located in the Edong district, which represents the westernmost and largest region within the Middle–Lower Yangtze River Metallogenic Belt (YRMB) (Fig. 1). Previous studies are focused on the geological setting, geochemistry of intrusive rocks, Sr–Nd isotopic data of granitoids and geochronology of ore deposits (Li et al., 2009, 2014; and references therein; Mao et al., 2011; Xie et al., 2016; Zhou et al., 2015; and Supplementary materials therein). However, some debates still surround the origin of magnetite–rich ores that have been interpreted to represent either magnetite–rich skarn or an iron–rich magma intruding into carbonate rocks.

The main ore mineral, magnetite, thus provides an opportunity to examine the genesis of the Tieshan Fe–Cu deposit. In this study, LA–ICP–MS is used to obtain *in–situ* trace elemental composition of magnetite. The data are used to elucidate the processes responsible for mineralization in the Tieshan Fe–Cu deposit.

2. Regional geological setting

The YRMB is located on the eastern part of the Yangtze Craton and along the southeastern margin of the North China Craton and the Dabie Orogenic Belt, which is bounded by the Xiangfan–Guangji Fault (XGF) to the northwest, the Tan–Lu regional strike–slip Fault (TLF) to the northeast and the Yangxin–Changzhou Fault (YCF) to the south (Fig. 1). It comprises seven ore deposit districts, including Edong, Jiurui, Anqing, Luzong, Tongling, Ningwu and Ningzhen, cropping out from west to east. Numerous ore deposits have been reported in this region, such as porphyry and porphyry–related skarn and stratabound deposits, being one of the most important Cu–Fe–Au–Mo–producing regions of China for the past three decades (Li et al., 2014; Mao et al., 2011; Pan and Dong, 1999; Shu et al., 1992; Xie et al., 2016; Zhou et al., 2015; and references therein).

The Edong district is located in the westernmost part of the YRMB, encompassing over 800 km^2 of igneous rocks and more than 70 porphyry–skarn and skarn Cu–Fe–Au–(Mo–W) deposits, related to Jurassic–Cretaceous plutons (Li et al., 2010, 2014; Shu et al., 1992; Wang et al., 2014a,b; Xie et al., 2011, 2015, 2016; Zhou et al., 2015) (Fig. 2). In this district, Cambrian to Middle Triassic marine sedimentary rocks and flysch successions are over 6000 m thick. Late Triassic to Cenozoic continental sediments and Early Cretaceous volcanic rocks comprise its stratigraphy. Early Cretaceous volcanic rocks resulted from extensive magmatism that formed a volcanic association ranging from basalts to rhyolites. This association is more than 2000 m thick and mostly localized in Jinniu basin covering today a 200 km^2 outcrop region (Fig. 2) (Bureau of Geology and Mineral Resources of Hubei Province, 1990; Shu et al., 1992).

As shown in Fig. 2, there are six plutons in the Edong district: (1) the Echeng granite and monzonite in the northern part, covering 85 km^2 in outcrop; (2) the Tieshan diorite and quartz diorite in the northwestern part, covering 140 km^2 in outcrop; (3) the Jinshandian quartz monzonite and monzogranite in the western part, covering 16 km^2 in outcrop; (4) the Lingxiang diorite and quartz diorite in the southwestern part, with an outcrop area of 54 km^2; (5) the Yangxin quartz diorite with minor granodiorite in the eastern part, with an outcrop area of 215 km^2 and (6) the Yinzu quartz diorite in the southernmost part, with an outcrop area of 90 km^2 (Shu et al., 1992). In addition, there are more than 100 small granite and granodiorite porphyry stocks and a number of dikes (diabase,

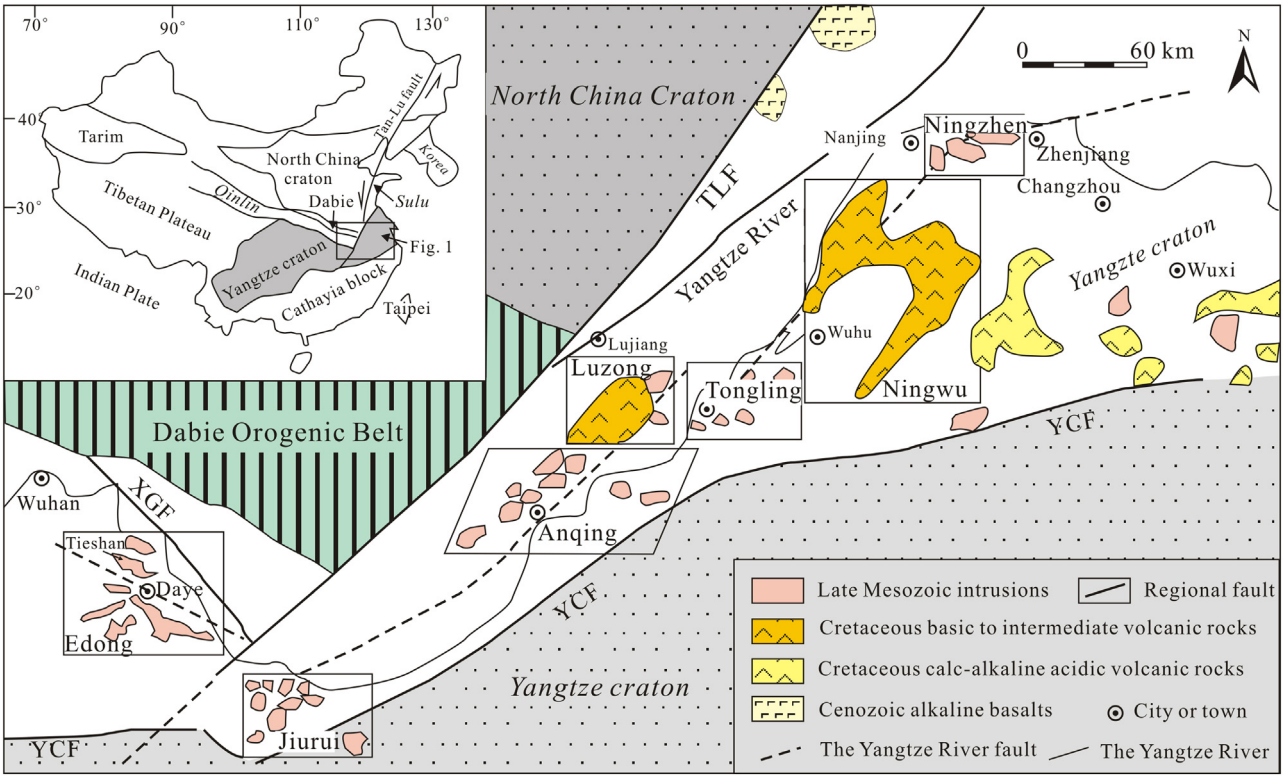

Fig. 1. Simplified geological map of the Middle–Lower Yangtze River Metallogenic Belt (YRMB), modified after Zhai et al. (1992, 1996). Abbreviations: TLF: Tan–Lu Fault, YCF: Yangxin–Changzhou Fault, XGF: Xiangfan–Guangji Fault.

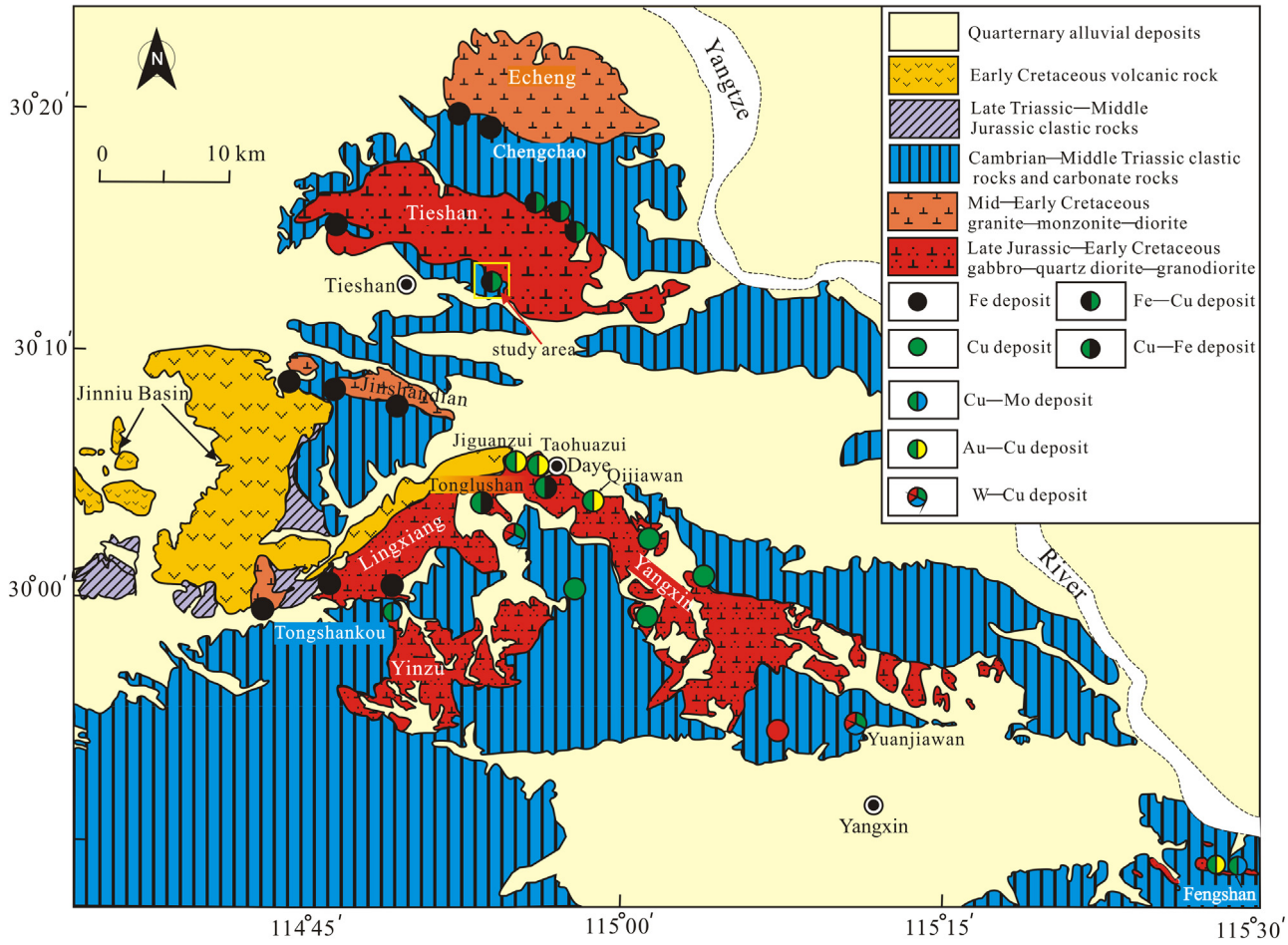

Fig. 2. Geological map of the Edong district, illustrating the distribution of main types of mineral deposits (modified after Li et al. (2008, 2009, 2014), Shu et al. (1992), and Xie et al. (2011, 2015)).

Table 1
The main characteristics of each ore body in the Tieshan Fe–Cu deposit.

Ore body	Location	Morphology	Length (m)	Down dip (m)	Thickness (m)	Occurrence		Elevation (m)
						Trend	Dip (°)	
Tiemenkan	Contact between the diorite and dolomitic marbles	lenticular or irregular	700	100–400	10–67	NNE (upper part) SSW (lower part)	35–87	+120–−300
Longdong	Contact between the diorite and dolomitic marbles	stratiform–like	600	150–450	10–55	SW	40–90	+190–−430
Jianlinshan	Contact between the diorite and dolomitic marbles	lenticular	750	10–420	20–80	NNE (east part) SSW (west part)	0–20	+92–−160
Xiangbishan	Contact between the quartz diorite or biotite pyroxene diorite and dolomitic marbles	lenticular	872	30–245	20–50	NE	10–60	+160–−430
Shizishan	Contact between the quartz diorite or biotite pyroxene diorite and marbles/dolomitic marbles	lenticular or wedge	430	80–610	30–150	NE (upper part) SW (deep part)	75–90	+170–−425
Jianshan	West part: contact of marble xenoliths	stratiform–like	520	320–620	40–120	NE (upper part) SW (deep part)	50–70	+160–−390
	East part: contact between the quartz diorite or biotite pyroxene diorite and dolomitic marbles	saccate	400	100–250	10–60	NE	35–45	+226–−142

Note: Summarization from Geological Team 609, Introduction to Central South Geo–exploration Institute.

diorite, monzonite and syenite) crop out, and surround or cut the plutons. Geochemical and Sr–Nd isotopic studies indicate that these intrusions are probably generated by partial melting of an enriched mantle that was previously metasomatized by slab–related melts of an ancient subduction system (Li et al., 2009; Shu et al., 1992; Wang et al., 2014a,b; Xie et al., 2008, 2015).

3. Geology of the Tieshan deposit

The Tieshan Fe–Cu deposit is located 114°54′43″ E and 30°13′10″ N, in the south of the Tieshan pluton (Fig. 2). The deposit comprises of several individual ore bodies and has estimated reserves of 160 Mt Fe with an average of grade of 52.1 wt.%

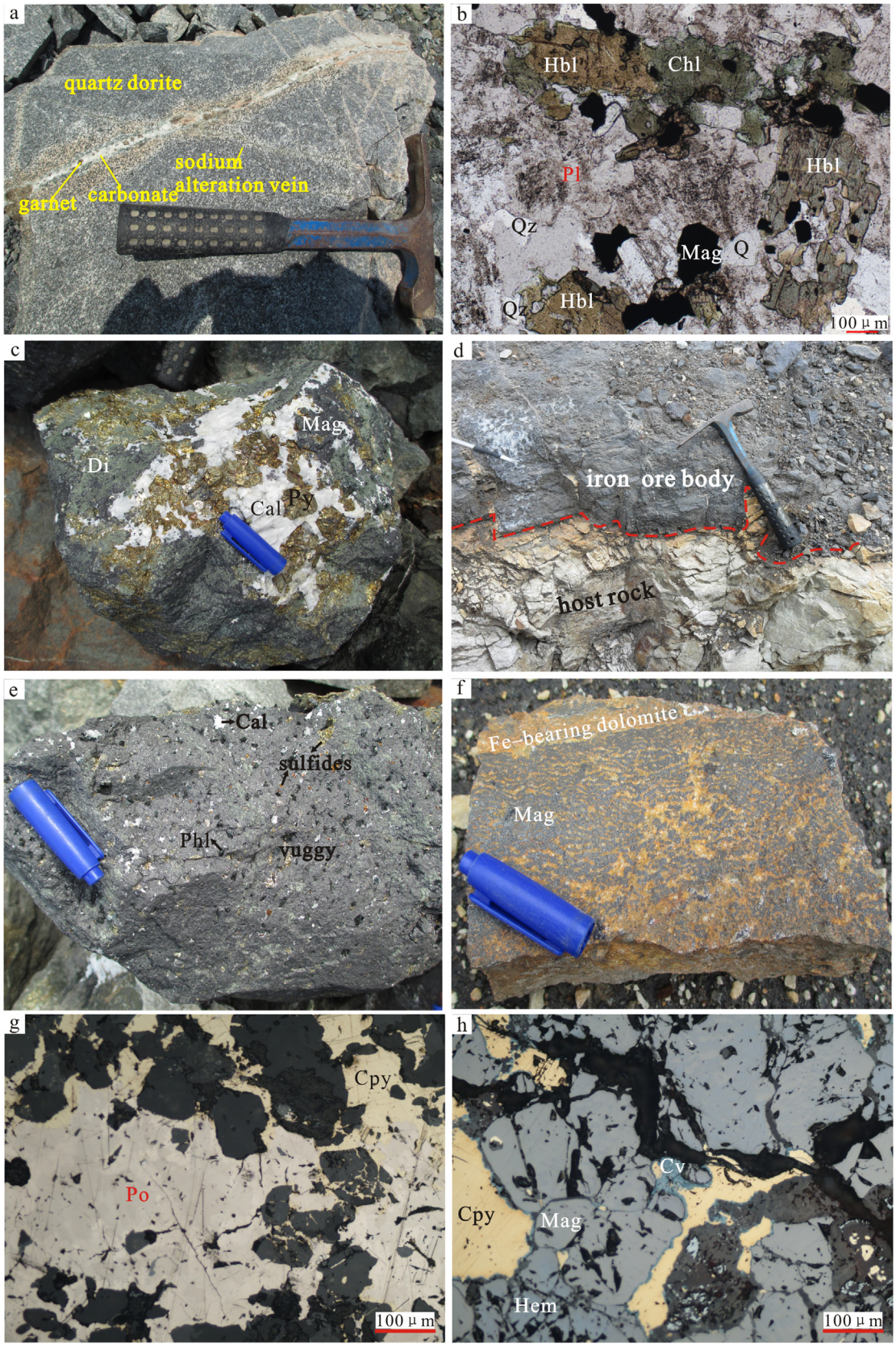

Fig. 3. Hand specimens and photomicrographs of the Tieshan Fe–Cu deposit. (a) Sodium alteration as veins in quartz diorite, with euhedral garnet in later carbonate vein from the Jianshan ore body. Hand specimen photograph. (b) Typical appearance of quartz diorite from the Xiangbishan ore body. Subhedral–anhedral hornblende, with pleochroism, and altered to chlorite in part of the mineral grain. Colorless anhedral quartz and plagioclase with polysynthetic twinning. Magnetite is opaque. Plain–polarized light. (c) Magnetite appearance with later anhedral pyrite and calcite metasomatized from the Jianshan ore body. Hand specimen photograph. (d) Magnetite ore body of sharp contact with host rocks and with very scarce or no skarn minerals. Hand specimen photograph. (e) Magnetite ores with amounts of vuggy, filling with sulfides, calcite and phlogopite in later mineralization stages. Hand specimen photograph. (f) Banded magnetite (dark color) with Fe–bearing dolomite (ocher color) from the Xiangbishan ore body.

Table 2
Electron microprobe analysis (wt.%) of magnetite from the Tieshan Fe–Cu deposit, Eastern China.

Sample	Spot No.	SiO_2	TiO_2	Al_2O_3	Cr_2O_3	Fe_2O_3	FeO	MnO	MgO	CaO	NiO	TOTAL
XBS–2	XBS2–1	0.06	0.10	0.26	b.d.	70.6	27.3	0.24	2.63	0.00	0.04	101.2
	XBS2–2	0.11	0.05	0.39	b.d.	70.7	27.1	0.21	2.83	0.00	0.08	101.5
	XBS2–3	0.23	0.04	0.46	b.d.	69.7	26.9	0.20	2.86	0.00	0.05	100.4
	XBS2–5	0.40	0.07	0.74	b.d.	69.5	27.0	0.23	3.13	0.00	0.05	101.1
	XBS2–7	0.82	0.09	0.59	b.d.	68.5	27.5	0.19	3.12	0.05	0.05	100.9
	XBS2–8	0.16	0.05	0.40	b.d.	70.1	26.8	0.23	2.87	0.00	0.08	100.7
	XBS2–9	0.07	0.08	0.62	b.d.	70.0	26.6	0.23	3.02	0.00	0.03	100.7
	XBS2–10	0.08	0.06	0.35	b.d.	70.7	27.1	0.24	2.76	0.00	0.06	101.4
XBS–5	XBS5–1	0.09	0.09	0.26	b.d.	69.4	28.6	0.13	1.69	0.00	0.06	100.3
	XBS5–2	0.06	0.07	0.17	b.d.	69.5	28.6	0.11	1.67	0.00	0.05	100.2
	XBS5–3	0.31	0.07	0.28	b.d.	69.3	29.0	0.10	1.77	0.00	0.04	100.9
	XBS5–5	0.77	0.12	0.34	b.d.	68.1	29.2	0.16	1.91	0.08	0.06	100.7
	XBS5–6	0.14	0.05	0.17	b.d.	68.8	28.8	0.13	1.40	0.00	0.04	99.5
	XBS5–7	0.11	0.05	0.32	b.d.	69.6	28.6	0.10	1.76	0.00	0.03	100.6
	XBS5–9	0.62	0.08	0.35	b.d.	68.5	29.0	0.13	1.92	0.03	0.06	100.7
	XBS5–10	0.23	0.06	0.25	b.d.	69.7	29.1	0.17	1.61	0.00	0.05	101.2
JS–10	JS10–1	0.10	0.10	0.39	b.d.	68.6	30.3	0.11	0.66	0.00	0.03	100.3
	JS10–2	0.10	0.11	0.35	b.d.	68.2	30.1	0.14	0.59	0.00	0.05	99.6
	JS10–3	0.07	0.14	0.45	b.d.	69.0	30.3	0.17	0.73	0.00	0.05	100.9
	JS10–4	0.08	0.13	0.31	b.d.	69.1	30.5	0.17	0.56	0.00	0.05	100.9
	JS10–5	1.32	0.10	0.94	b.d.	65.5	30.7	0.10	1.31	0.18	0.08	100.2
	JS10–6	0.53	0.08	0.50	b.d.	66.8	30.0	0.15	0.87	0.00	0.06	99.0
	JS10–7	0.08	0.09	0.34	b.d.	68.8	30.2	0.15	0.63	0.00	0.04	100.3
	JS10–8	1.66	0.15	0.67	b.d.	64.8	30.9	0.08	1.35	0.30	0.05	100.0
	JS10–9	0.85	0.07	0.54	b.d.	67.0	30.6	0.14	1.01	0.06	0.03	100.3
	JS10–10	0.23	0.09	0.46	b.d.	68.1	30.4	0.15	0.62	0.00	0.05	100.1
JS–17	JS17–1	0.47	0.09	0.74	b.d.	67.8	30.3	0.31	0.90	0.00	0.07	100.7
	JS17–2	0.39	0.06	0.51	b.d.	67.9	31.0	0.35	0.32	0.00	0.05	100.6
	JS17–3	1.32	0.11	1.21	b.d.	64.8	30.8	0.40	1.13	0.08	0.02	99.9
	JS17–4	0.73	0.10	0.30	b.d.	68.0	29.3	0.10	1.87	0.01	0.04	100.5
	JS17–5	0.57	0.09	0.60	0.01	67.4	31.1	0.32	0.43	0.00	0.05	100.6
	JS17–6	0.30	0.10	0.56	b.d.	67.7	31.1	0.28	0.23	0.00	0.01	100.3
	JS17–7	1.37	0.13	0.93	b.d.	65.4	30.9	0.33	1.17	0.18	0.06	100.5
	JS17–8	0.07	0.08	0.31	b.d.	69.2	30.2	0.28	0.64	0.00	0.07	100.9
	JS17–9	0.51	0.10	0.62	b.d.	67.2	30.9	0.34	0.45	0.02	0.04	100.2
	JS17–10	0.39	0.09	0.55	b.d.	67.5	31.1	0.20	0.32	0.00	0.06	100.2

Note: "b.d." below the limit of detection; Oxygen was calculated from cation stoichiometry, and the chemical formula was normalized to 32 O atoms.

Fe, as well as 0.67 Mt Cu with an average grade of 0.57 wt.% and 48 t Au (Li et al., 2014; Xie et al., 2015).

The Tieshan pluton intrudes carbonates of the Lower Triassic Daye Formation. The Daye Formation is composed of limestone, dolomite, shale and marl (Shu et al., 1992). Within a few hundred meters of the intrusions, these carbonate rocks are thermally metamorphosed to marble and dolomitic marble. The Tieshan pluton consists of six intrusive bodies, which are, from a temporal order, syenodiorite, gabbroic diorite, monzodiorite, granodiorite and quartz diorite or monzodiorite (Li et al., 2014). The modal mineral composition of quartz diorite is 55% plagioclase, 15% K–feldspar, 10% quartz, 15% hornblende and 5% biotite (Fig. 3a, b) (Qu et al., 2012). Recently, zircon U–Pb and phlogopite (cogenetic with ore minerals) $^{40}Ar/^{39}Ar$ dating help us to better understand the relationship between the magmatism and mineralization, indicating age of deposits from 148 ± 1.0 Ma to 137 ± 2 Ma (Li et al., 2009, 2014; Xie et al., 2015).

The Tieshan Fe–Cu deposit comprises of six ore bodies, which are Tiemenkan, Longdong, Jianlinshan, Xiangbishan, Shizishan and Jianshan, from west to east, and ore bodies are predominantly located along the contact between diorite/quartz diorite and marbles/dolomitic marbles (Fig. 4a, b). All ore bodies crop out, except Jianlinshan, which is a blind ore body and mined underground now (Shu et al., 1992). The ore bodies have lenticular or podiform shape, being 400–872 m long, 10–150 m thick and continuous for 245–620 m down dip from 92 m to −430 m in elevation (Shu et al., 1992). The detailed geological characteristics of each ore body are summarized in Table 1.

The Tieshan deposit consists of two main types of iron mineralization: (1) magnetite ores in the contact associated with typical skarn minerals (Fig. 3c) and (2) magnetite ores with amounts of vuggy, filling with sulfides, calcite and phlogopite, and of sharp contact with host rocks, having very scarce or no skarn minerals (Fig. 3d, e), with the former being economically much more important.

The mineralogy of each ore body is similar, with ore minerals characterized by magnetite, hematite, chalcopyrite, bornite, marcasite, pyrrhotite, and siderite, *etc*., and gangue minerals characterized by silicates and carbonates, including diopside, garnet, scapolite, phlogopite, actinolite, chlorite, albite, plagioclase, tremolite, and epidote. This assemblage is frequently overprinted by quartz, calcite, ankerite, anhydrite and fluorite (Fig. 3f–h).

4. Sampling and analytical methods

Four samples were collected from open pit for this study (the location of each sample shown in Fig. 4a). Sample XBS−2 and XBS−5 are massive magnetite ores, collected from the Xiangbishan ore

Hand specimen photograph. (g) The main sulfide minerals– pyrrhotite and chalcopyrite from the Jianshan ore body. Reflected light image, plain–polarized light. (h) The microscopic characteristics of magnetite ore samples for analysis of the Tieshan Fe–Cu deposit. Magnetite (brown hue) is the main mineral, paragenesis with hematite (light blue gray hue) and minor chalcopyrite (with covellite surrounded). Reflected light image, plain–polarized light. Abbreviations: Cal: Calcite; Chl: Chlorite; Cv: covellite; Di: Diopside; Hbl: Hornblende; Hem: Hematite; Mag: Magnetite; Phl: Phlogopite; Pl: plagioclase; Po: pyrrhotite; Py: pyrite; Qz: Quartz. Abbreviations based on Whitney and Evans (2010). (For interpretation of the references to colour in this figure legend, the reader is referred to the web version of this article.)

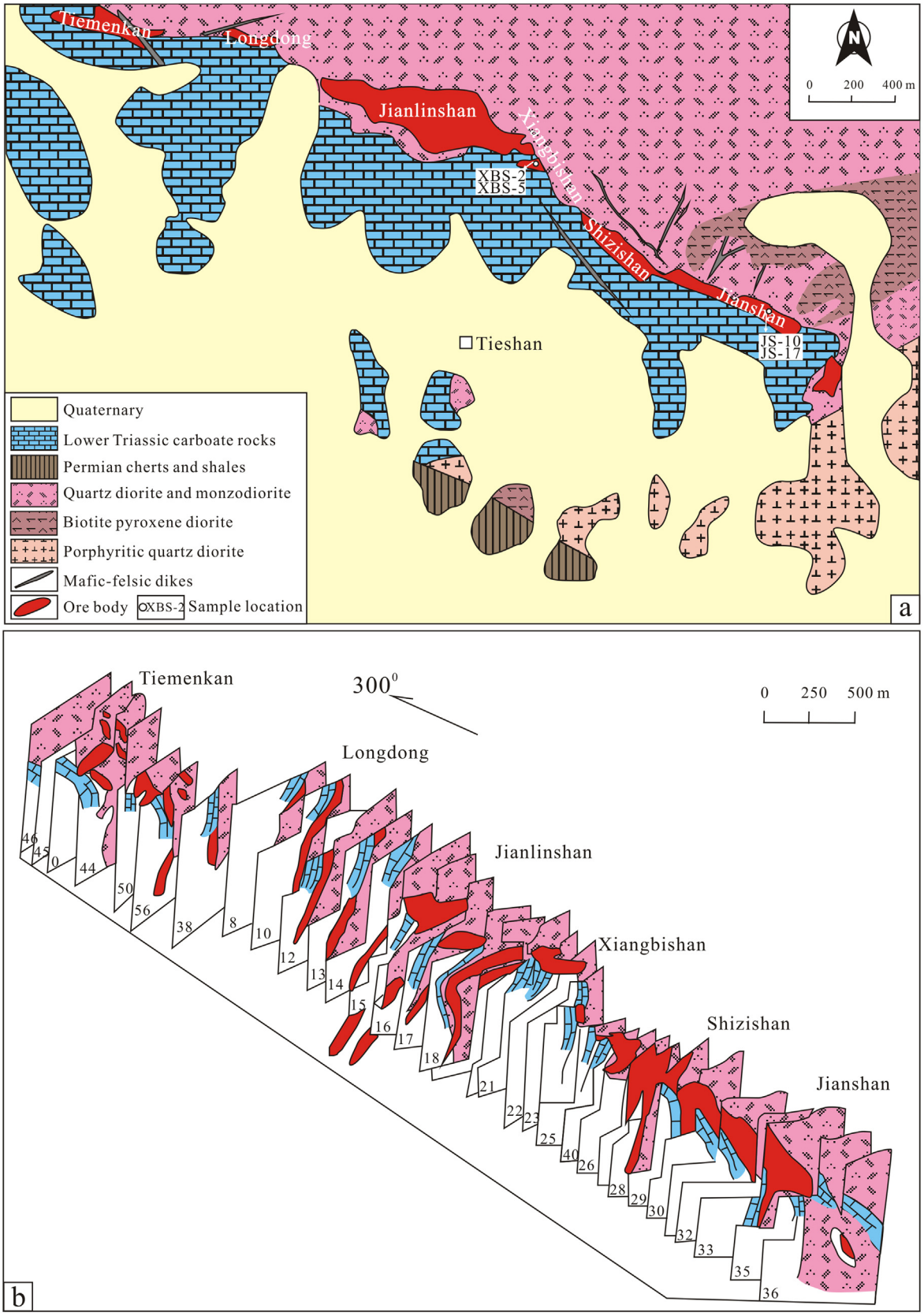

Fig. 4. (a) Simplified geological map of the Tieshan Fe–Cu deposit (modified after Shi et al. (1982)). (b) Sections of the Tieshan Fe–Cu deposit (modified after Liu et al. (2007)).

body. The mineralogy of sample XBS–2 and XBS–5 are similar, comprising magnetite, hematite, chalcopyrite, pyrrhotite, pyrite, phlogopite, chlorite, and siderite. Sample JS–10 and JS–7 are magnetite ores with minor sulfides, collected from the Jianshan ore body, consisting of magnetite, hematite, chalcopyrite, pyrrhotite and pyrite (Fig. 3h).

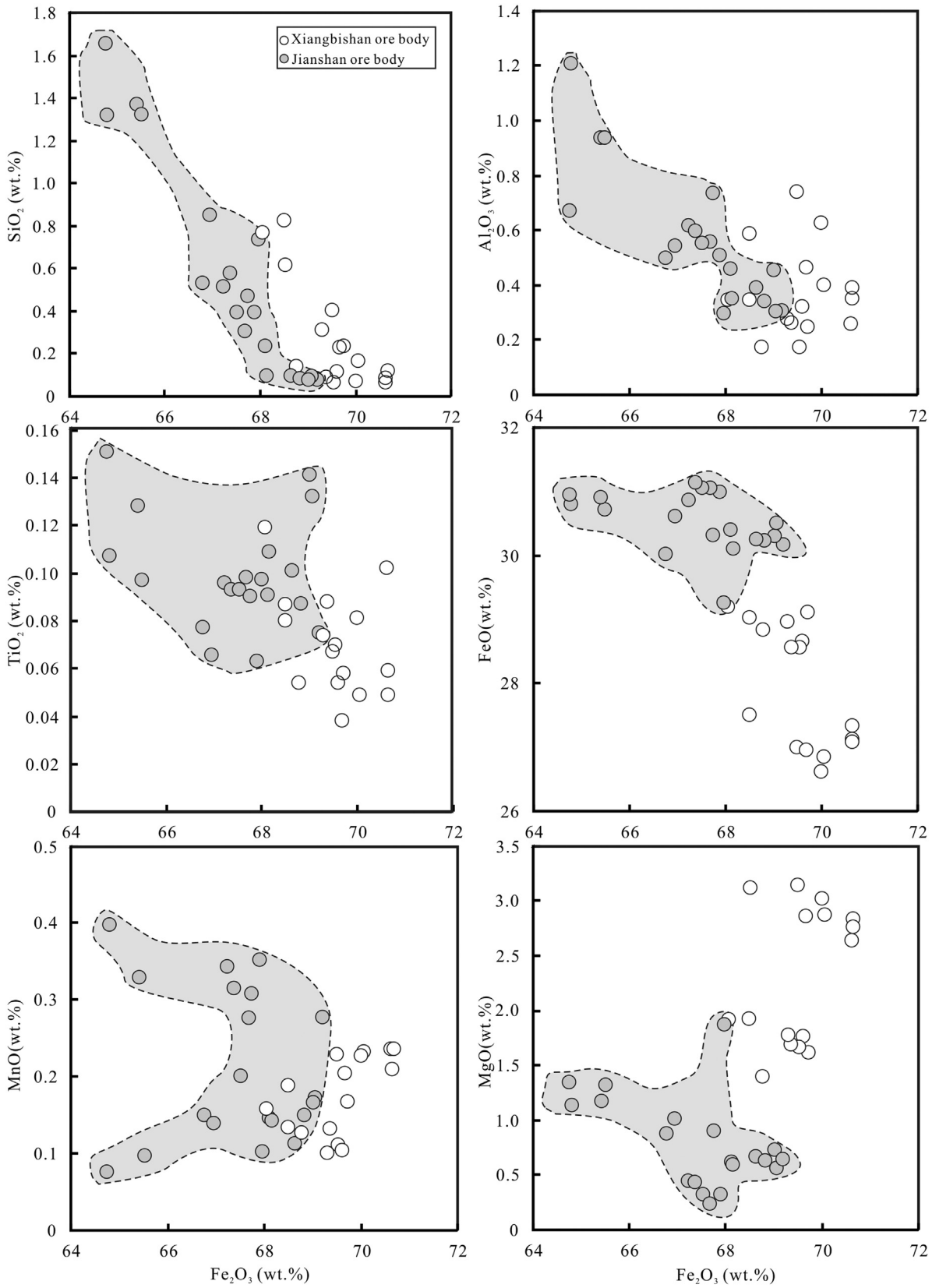

Fig. 5. Scatter plots illustrating the relation between Fe_2O_3 and other element contents for magnetite from the Tieshan deposit.

All samples were prepared as polished thin sections and subsequently examined using optical microscopy to characterize the mineralogical and textural relationships, with an emphasis on the occurrence, morphology and texture of magnetite. The composition of magnetite were analyzed by electron microprobe analysis (EMPA) at the State Key Laboratory of Geological Processes and Mineral Resources, China University of Geosciences (Wuhan). EMPA of magnetite was performed using a JXA–8100. Standards

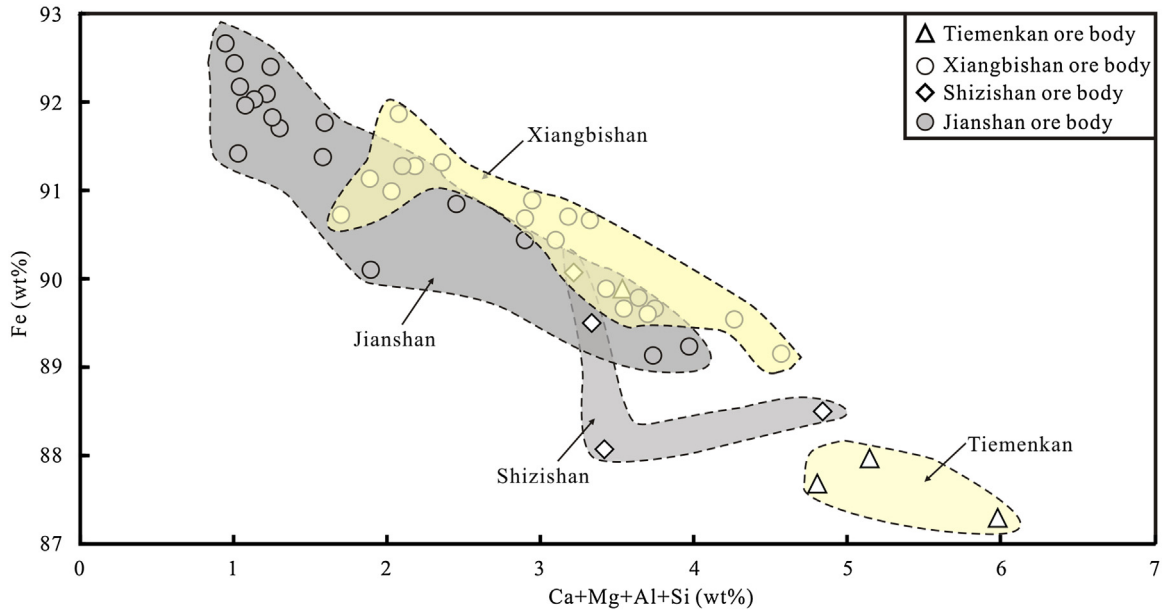

Fig. 6. Diagram between Fe content (wt.%) and Ca + Mg + Al + Si content (wt.%) of magnetite from the Tieshan Fe–Cu deposit. Note: data of the Tiemenkan and Shizishan ore bodies from Zhao (1990), all other data from this study.

and unknowns were analyzed using a 10 μm beam diameter, an accelerating voltage of 15 kV, and an absorbed beam current of 20 nA. The following standards were used: Fe (magnetite), Cu (copper), Mg (forsterite), Al (kyanite), Si (almandine), Mn (spessartine), Ca (diopside), Ti (titanite), Na (jadeite), K (orthoclase), Ni (nickel), Cr (chromium oxide). The data were reduced using the ZAF correction method. It describes a procedure in which corrections for atomic number effects (Z), absorption (A) and fluorescence (F) are calculated separately from suitable physical models.

The trace elemental geochemistry of magnetite from the Tieshan Fe–Cu deposit has been investigated using *in situ* laser ablation inductively coupled plasma–mass spectrometry (LA–ICP–MS), performed at the National Research Center for Geoanalysis (NRCG), Chinese Academy of Geological Sciences, Beijing. A New Wave NWR–193 laser ablation system coupled to a Thermo Element II mass spectrometer was used. Helium, as a carrier gas, and argon, as a makeup gas, were mixed *via* a T–connector prior to the entering of the ICP. Each analysis was performed by laser wave of 193 nm, laser spot size of 35 μm in diameter and frequency of 10 Hz, beam energy of ~2 mJ per pulse and density of 23–25 J/cm^2. Each analysis started with 15 s for gas blank, followed by data acquisition of 40 s from the sample and ongoing 15 s for cleaning the system when laser ablation stopped. The total analytical time for each analysis is 70 s. The analytical parameters of the gas velocity for the instrumentation are: 16 L/min for cooling gas flow (Ar), 0.73 L/min for auxiliary gas flow (Ar), 0.58 L/min for carrier gas flow (He), 0.819 L/min for sample gas flow. Element contents were calibrated using NIST 612 as the external calibration standard and using ^{57}Fe determined as an internal standard to validate the results obtained of trace element for magnetite. Data processing is performed using the program Excel. Detailed description of instrumentation and analytical and calibration procedures were given by Hu et al. (2008, 2011).

5. Results

5.1. Composition of magnetite as analyzed by EMPA

Results of EMPA for all samples are presented in Table 2. Oxygen was calculated from cation stoichiometry, and the chemical formula was normalized to 32 oxygen atoms. Data illustrate low Al_2O_3 (0.17–1.21 wt.%, aver = 0.48 wt.%), SiO_2 (0.06–1.66 wt.%, aver = 0.43 wt.%), FeO (26.6–31.1 wt.%, aver = 29.4 wt.%), but higher Fe_2O_3 (64.8–70.7 wt.%, aver = 68.4 wt.%). The Cr_2O_3 content was below the limit of detection. Higher Fe_2O_3 and MgO contents occur in the samples from the Xiangbishan ore body than those from the Jianshan ore body (Fig. 5). In addition, SiO_2, Al_2O_3 and MnO contents occupy a wider range in the Jianshan ore body than those in Xiangbishan ore body.

A diagram relating the Fe content against Ca + Mg + Al + Si atoms was plotted (Fig. 6). Data of magnetite from the western Tiemenkan ore body and the central Shizishan ore body were analyzed by Zhao (1990). From the western Tiemankan ore body to the eastern Jianshan ore body of the Tieshan deposit, FeO content increases and CaO + MgO + Al_2O_3 + SiO_2 content decreases, which may illustrate that the environment in which the magnetite formed (magma or fluids) became more mafic (esp. more Ca and Mg rich) from the western Tiemenkan ore body to the eastern Jianshan ore body. This may be related to the occurrence of rather mafic biotite pyroxene near the Jianshan ore body (Fig. 4a). This may, however, also imply that the Jianshan ore body formed as an exoskarn, replacing dolomitic marble whereas the Xiangbishan ore body may have, in contrast, have formed as a contact skarn.

5.2. Trace element chemistry of magnetite by LA–ICP–MS

A total of 178 grains of magnetite from the four magnetite samples were analyzed by LA–ICP–MS. Results illustrate that magnetite from the Tieshan Fe–Cu deposit contains substantial V, Cr, Co, Ni, Cu, Zn, Ga, Ge, and Sn, but these concentrations vary significantly, as illustrated by the concentration of V (13.61–542.36 ppm), Cr (0.003–383.96 ppm), Co (11.12–187.55 ppm) and Ni (0.19–147.41 ppm), *etc*. In addition, there is a spatial variation within individual magnetite grains (Appendix I), which has been observed in many iron deposits, such as, Los Colorados iron oxide–apatite deposit, Chile (Knipping et al., 2015a, 2015b; Reich et al., 2016), porphyry Cu–Mo–Au deposits in British Columbia, Canada (Canil et al., 2016) and Chengchao iron deposit, China (Hu et al., 2014), *etc*.

In order to compare the large variations of trace element in magnetite from the two ore bodies, multi–element variation diagrams

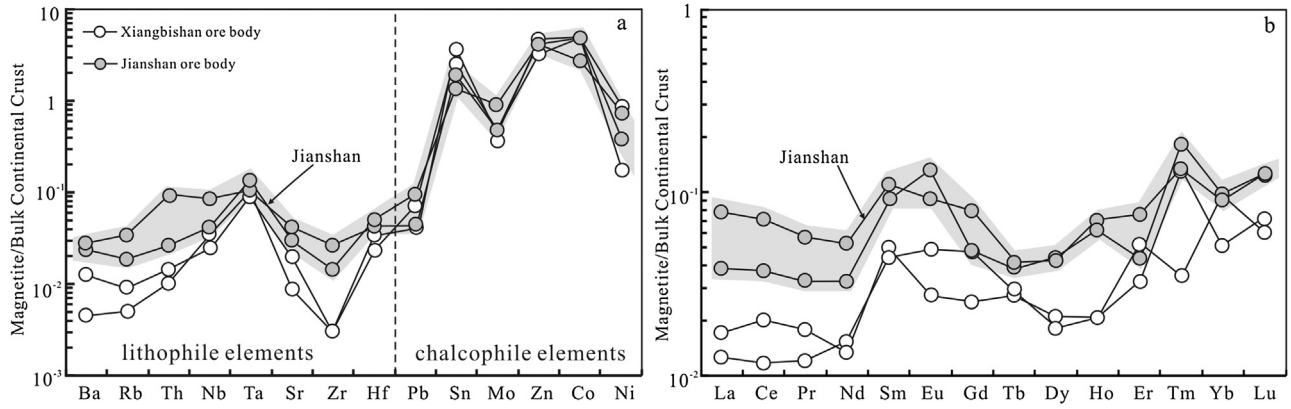

Fig. 7. Multi–element variation diagrams of trace element concentrations in the Tieshan Fe–Cu deposit (a) and for REE element (b). Normalized to bulk continental crust using values from Rudnick and Gao (2003).

of trace element concentrations are plotted (Fig. 7). Two groups are distinguished, namely lithophile elements (Ba, Rb, Th, Nb, Ta, Sr, Zr, Hf) and chalcophile elements (Pb, Sn, Mo, Zn, Co, Ni). Normalization to bulk continental crust, using values from Rudnick and Gao (2003), is preferred to normalizing to primitive mantle because by the time magnetite crystallizes the magma has evolved to a diorite or granodiorite composition that is more similar in composition to bulk continental crust than to primitive mantle.

Magnetite from the Jianshan ore body has higher lithophile elements and REE contents, but lower chalcophile elements concentrations than those from the Xiangbishan ore body (Fig. 7), which probably due to the different forming environment of magnetite in the two ore bodies. In general, chalcophile elements concentrations are higher than lithophile elements in magnetite from the Tieshan Fe–Cu deposit. In addition, there is a pronounced difference in the lithophile elements concentrations between the two ore bodies. Higher Ba, Rb, Th, Sr, Zr and Hf elements concentrate in the Jianshan ore body than those in the Xiangbishan ore body (Fig. 7a).

6. Discussion

6.1. Magnetite as a discriminator for ore genesis

Ore genesis of the Tieshan Fe–Cu deposit is controversial with big debate on the magnetite ore bodies, which have sharp contact with host rocks and amounts of vuggy in ores. Some researchers proposed that the high grade, magnetite–dominated sharp bodies were directly crystallized from iron oxide melts (Shi et al., 1982; Zhai et al., 1996). However, some other researchers insist that these sharp bodies were caused by replacement along fractures penetrating the Triassic carbonates, or being precipitated from iron–rich fluids facilitated by fluid immiscibility due to an abrupt decrease in pressure/temperature of the fluids when they fluxed into the fractures (Zhao, 1993).

In the diagram Ca + Al + Mn and Ti + V of Dupuis and Beaudoin (2011) (Fig. 8), magnetite occupies the skarn field. This strongly suggests that the magnetite ores formed by hydrothermal replacement of carbonate host rocks, while not from iron oxide melts. In addition, it is obvious that the trace element concentrations have a

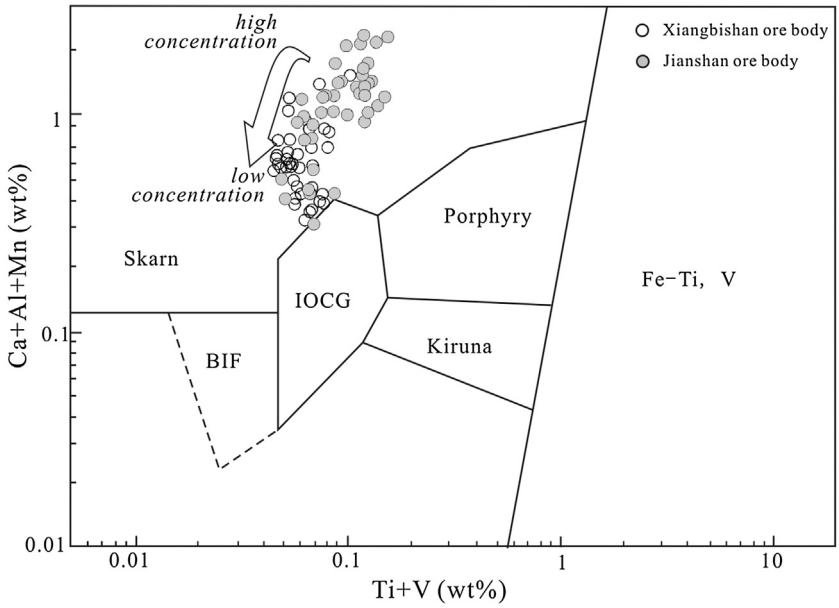

Fig. 8. Ca + Al + Mn *vs.* Ti + V discrimination diagram for LA–ICP–MS data of magnetite from the Tieshan Fe–Cu deposit. Reference fields are from Dupuis and Beaudoin (2011). Abbreviations: BIF: banded iron formation; Skarn: Fe–Cu skarn deposits; IOCG: iron oxide–copper–gold deposits; Porphyry: porphyry Cu deposits; Kiruna: Kiruna apatite–magnetite deposits; Fe–Ti, V: magmatic Fe–Ti–oxide deposits.

trend from high to low (Fig. 8), which reflects a down–temperature precipitation trend.

The major element mineral chemistry of magnetite varies greatly between different ore–forming environments. This renders magnetite useful to place constraints on ore genesis (Xu and Shao, 1979). Almost all the data presented here for magnetite from the Tieshan deposit fall into the skarn field and hydrothermal superimposition field in the TiO_2–Al_2O_3–MgO ternary diagram that was originally proposed by Wang (1987) (Fig. 9). Magnetite from the western Tiemenkan ore body plots in the hydrothermal superimposition field; magnetite from the central Xiangbishan ore body plots in the magnesium skarn field, those from the central Shizishan ore body plots in both the magnesium skarn field and transition field. Magnetite from the eastern Jianshan ore body plots in the calcium skarn field, magnesium skarn field and transition field. In general, from the western part to the eastern part of the Tieshan Fe–Cu deposit, the composition of magnetite becomes more and more variable, illustrated by the fact of the data (Fig. 9).

6.2. Precipitation of magnetite from hydrothermal fluids

The mineral chemistry of magnetite deposited from hydrothermal fluids is mostly controlled by: (1) fluid composition, (2) temperature, (3) pressure, (4) cooling rate, (5) oxygen or sulfur fugacity, (6) silica activity (Nadoll et al., 2014; and references there in) and (7) composition of host rocks (Nadoll, 2010). Several of these controls have evidently exceeded an important influence on the magnetite in different portions of the Tieshan deposit.

Magnetite of samples from the Xiangbishan ore body have higher Mg, but lower Mn content than those from the Jianshan ore body (Fig. 10a, b), which is due to the various lithography of host rock. The host rock in the Xiangbishan ore body was dolomitic marble, but hornfels and marble in the Jianshan ore body. In contrast, the range of Cu and Zn contents is similar for magnetite across the Tieshan deposit. This is attributed to very effective partitioning of these chalcophile elements into sulfide minerals rather than magnetite– and the abundance of co–existing sulfides in all ore bodies of the Tieshan deposit (Fig. 10c).

Titanium and V concentrations are a powerful tool to monitor for redox conditions and the influence of mafic materials on magnetite formation. Although vanadium has variable valence states in aqueous fluids, only V(III) can be easily incorporated into the magnetite structure (Bordage et al., 2011; Nadoll et al., 2014; Toplis and Corgne, 2002). Therefore, vanadium is preferably enriched in relatively reduced fluids. In contrast, Ti has only Ti(IV) in hydrothermal fluids and hence the partition coefficient is rather consistent between magnetite and fluids. Thus, magnetite formed from reduced fluids is expected to have Ti/V ratios lower than those formed from oxidized fluids. The Ti/V ratio of magnetite from the Xiangbishan ore body ranges from 1.32 to 5.24, with 2.70 as an average. The same ratio is between 1.31 and 10.34, with 4.84 as an average in magnetite from the Jianshan ore body, which indicating a relatively reduced depositional environment in the Xiangbishan ore body (Fig. 10d).

In addition, magnetite from the Xiangbishan ore body is also depleted in Ti, Pb, and Al, relative to magnetite from the Jianshan ore body (Fig. 10e, f). The incorporation of Ti and Al in magnetite is temperature dependent, with higher temperatures resulting in higher concentrations (Nielsen et al., 1994). This may tentatively, be used to suggest that the temperature of magnetite formation at the Jianshan ore body was higher than at the Xiangbishan ore body. In summary, mineral chemistry may suggest a lower temperature and lower oxygen fugacity (fO_2) for the formation of magnetite in the Xiangbishan ore body than in the Jianshan ore body.

7. Conclusion

Magnetite from the Tieshan Fe–Cu deposit is shown to contain a wide range of trace elemental concentrations. Data observed from

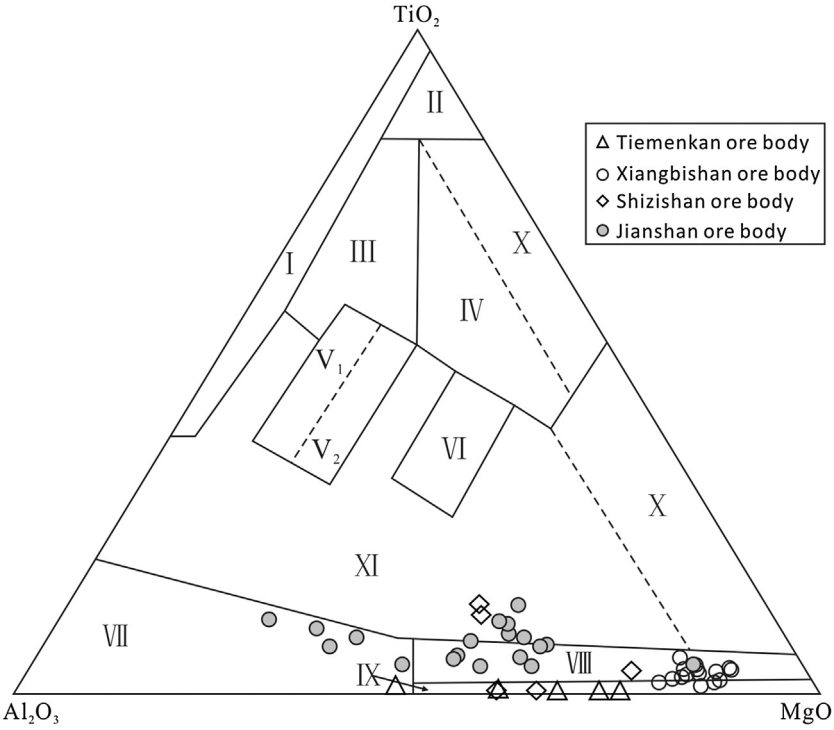

Fig. 9. Ternary diagram of TiO_2–Al_2O_3–MgO for magnetite from the Tieshan Fe–Cu deposit, allowing the discrimination of different ore–forming environments (Wang, 1987) I: granite field; II: basalt field; III: gabbro field; IV: peridotite field; V_1: amphibolite field; V_2: diorite field; VI: kimberlite field; VII: calcium skarn field; VIII: magnesium skarn field; IX: hydrothermal superimposition field; X: carbonate field; XI: transition field. Note: data of the Tiemenkan and Shizishan ore bodies from Zhao (1990), all other data from this study.

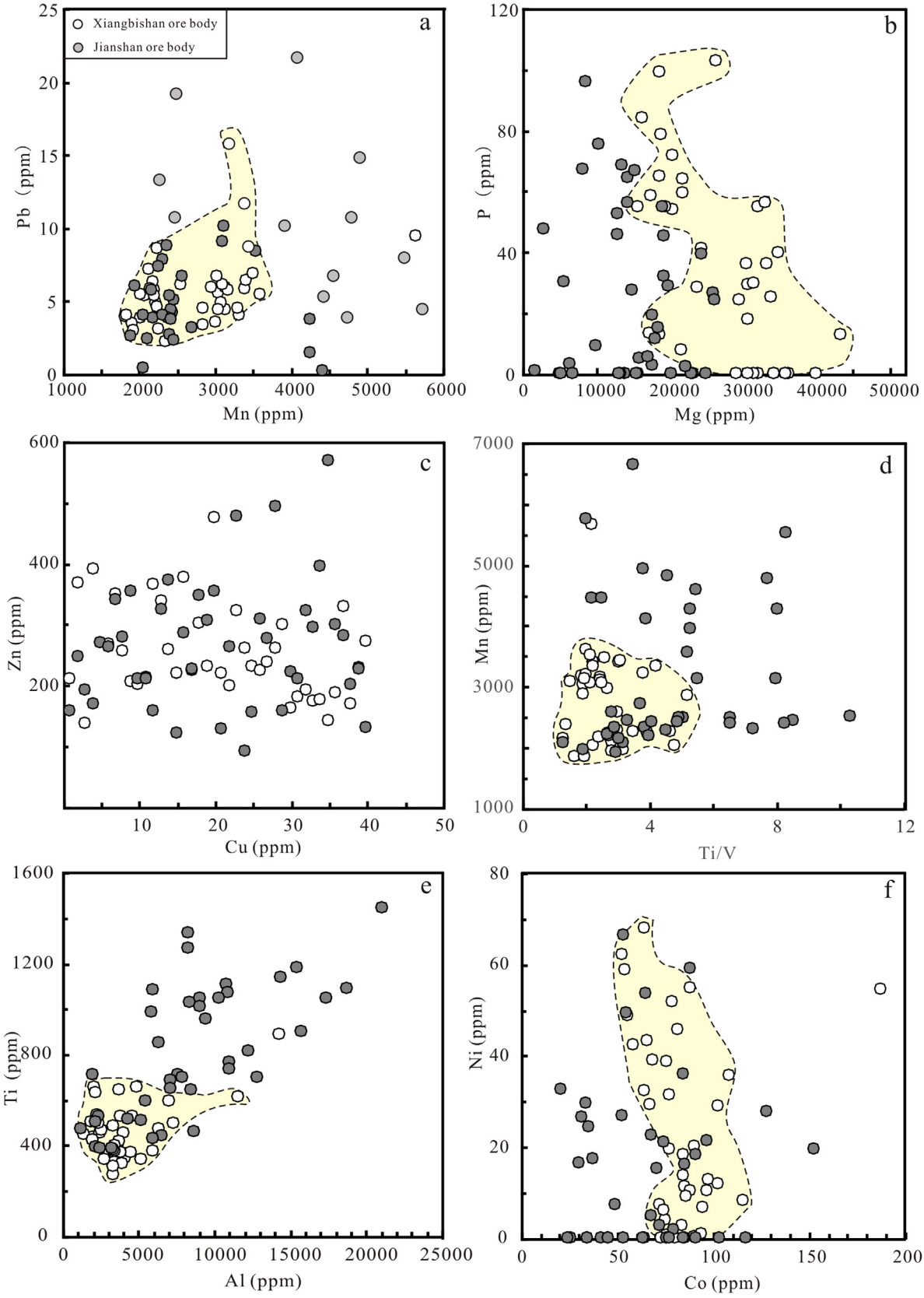

Fig. 10. Scatter plots of Mn *vs*. Pb, Mg *vs*. P, Cu *vs*. Zn, Ti/V *vs*. Mn, Al *vs*. Ti, Co *vs*. Ni for magnetite from the Xiangbishan and Jianshan ore bodies in the Tieshan Fe–Cu deposit.

LA–ICP–MS and EMPA analysis illustrate that magnetite from the Tieshan deposit formed by hydrothermal processes rather than iron oxide melts. However, data also reveal significant and systematic differences between different parts of the Tieshan deposit. These differences may be attributed to different controlling factors. Elevated Co, Ni and Mg contents in magnetite from the Xiangbishan

ore body likely reflected the influence of the abundance of dolomitic marble nearby. Low Ti/V ratio, Ti and Al contents illustrate a relatively low temperature and fO_2 during magnetite formation at the Xiangbishan ore body as compared to the Jianshan ore body, which shows clear down–temperature precipitation trend.

Acknowledgements

This study was supported by grants by the National Natural Science Foundation of China (No. 41272097), the China Geological Survey Project (No. 12120114016601), the Special Fund for Basic Scientific Research of Central Colleges, China University of Geosciences (Wuhan) (No. CUG120702), and the Teaching Laboratory Foundation of China University of Geosciences (Wuhan) (No. SKJ2015010, SKJ2015017). We are indebted to Prof. Jens Gutzmer for his beneficial suggestion, communication and revision for this paper. Comments and suggestions from anonymous reviewers and Editor-in-Chief Alex Deutsch greatly improved the quality of the paper.

Appendix A. Supplementary data

Supplementary data associated with this article can be found, in the online version, at http://dx.doi.org/10.1016/j.chemer.2016.11.002.

References

Bordage, A., Balan, E., De Villiers, J.P., Cromarty, R., Juhin, A., Carvallo, C., Calas, G., Raju, P.S., Glatzel, P., 2011. V oxidation state in Fe-Ti oxides by high-energy resolution fluorescence-detected X-ray absorption spectroscopy. Phys. Chem. Miner. 38, 449–458.

Bureau of Geology and Mineral Resources of Hubei Province, 1990. Regional Geology of Hubei Province, 1 st ed. Geological Publishing Housing, Beijing (in Chinese with English abstract).

Canil, D., Grondahl, C., Lacourse, T., Pisiak, L.K., 2016. Trace elements in magnetite from porphyry Cu-Mo-Au deposits in British Columbia, Canada. Ore Geol. Rev. 72, 1116–1128.

Carrew, M.J., 2004. Controls on Cu-Au Mineralisation and Fe Oxide Metasomatism in the Eastern Fold Belt. James Cook University, N.W Queensland, Australia, pp. 1–308.

Chen, W.T., Zhou, M.F., Li, X.C., Gao, J.F., Hou, K.J., 2015. In-situ LA-ICP-MS trace elemental analyses of magnetite: Cu-(Au Fe) deposits in the Khetri copper belt in Rajasthan Province, NW India. Ore Geol. Rev. 65 (Part (4)), 929–939.

Chung, D., Zhou, M.-F., Gao, J.-F., Chen, W.T., 2015. In-situ LA-ICP-MS trace elemental analyses of magnetite: the late Palaeoproterozoic Sokoman Iron Formation in the Labrador Trough, Canada. O re Geol. Rev. 65 (Part (4)), 917–928.

Dare, S.A.S., Barnes, S.-J., Beaudoin, G., 2012. Variation in trace element content of magnetite crystallized from a fractionating sulfide liquid, Sudbury, Canada: implications for provenance discrimination. Geochim. Cosmochim. Acta 88, 27–50.

Deer, W., Howie, R., Zussman, J., 1992. An Introduction to Rock-Forming Minerals, 2nd edn. Longman Harlow, Wiley New York.

Dupuis, C., Beaudoin, G., 2011. Discriminant diagrams for iron oxide trace element fingerprinting of mineral deposit types. Miner. Deposita 46, 319–335.

Hu, M.Y., He, H.L., Zhan, X.C., Fan, X.T., Wang, G., Jia, Z.R., 2008. Matrix normalization for in-situ multi-element quantitative analysis of zircon in laser ablation-inductively coupled plasma mass spectrometry. Chin. J. Anal. Chem. 36, 947–953 (in Chinese with English abstract).

Hu, M.Y., Fan, X.T., Stoll, B., Kuzmin, D., Liu, Y., Liu, Y., Sun, W., Wang, G., Zhan, X.C., Jochum, K.P., 2011. Preliminary characterisation of new reference materials for microanalysis: chinese geological standard glasses CGSG-1, CGSG-2, CGSG-4 and CGSG-5. Geostand. Geoanal. Res. 35, 235–251.

Hu, H., Li, J.-W., Lentz, D., Ren, Z., Zhao, X.-F., Deng, X.-D., Hall, D., 2014. Dissolution–reprecipitation process of magnetite from the Chengchao iron deposit: insights into ore genesis and implication for in-situ chemical analysis of magnetite. Ore Geol. Rev. 57, 393–405.

Huang, X.-W., Gao, J.-F., Qi, L., Zhou, M.-F., 2015. In-situ LA-ICP-MS trace elemental analyses of magnetite and Re-Os dating of pyrite: the Tianhu hydrothermally remobilized sedimentary Fe deposit, NW China. Ore Geol. Rev. 65 (Part (4)), 900–916.

Huang, X.-W., Gao, J.-F., Qi, L., Meng, Y.-M., Wang, Y.-C., Dai, Z.-H., 2016. In-situ LA-ICP-MS trace elements analysis of magnetite: the Fenghuangshan Cu-Fe-Au deposit, Tongling, Eastern China. Ore Geol. Rev. 72 (Part (1)), 746–759.

Knipping, J.L., Bilenker, L.D., Simon, A.C., Reich, M., Barra, F., Deditius, A.P., Lundstrom, C., Bindeman, I., Munizaga, R., 2015a. Giant Kiruna-type deposits form by efficient flotation of magmatic magnetite suspensions. Geology 43, 591–594.

Knipping, J.L., Bilenker, L.D., Simon, A.C., Reich, M., Barra, F., Deditius, A.P., Wälle, M., Heinrich, C.A., Holtz, F., Munizaga, R., 2015b. Trace elements in magnetite from massive iron oxide-apatite deposits indicate a combined formation by igneous and magmatic-hydrothermal processes. Geochim. Cosmochim. Acta 171, 15–38.

Li, J.W., Zhao, X.F., Zhou, M.F., Vasconcelos, P., Ma, C.Q., Deng, X.D., de Souza, Z.S., Zhao, Y.X., Wu, G., 2008. Origin of the Tongshankou porphyry-skarn Cu-Mo deposit, eastern Yangtze craton, Eastern China: geochronological, geochemical, and Sr-Nd-Hf isotopic constraints. Miner. Deposita 43, 315–336.

Li, J.W., Zhao, X.F., Zhou, M.F., Ma, C.Q., de Souza, Z., Vasconcelos, P., 2009. Late Mesozoic magmatism from the Daye region, eastern China U-Pb ages, petrogenesis, and geodynamic implications. Contrib. Mineral. Petrol. 157, 383–409.

Li, J.W., Deng, X.D., Zhou, M.F., Liu, Y.S., Zhao, X.F., Guo, J.L., 2010. Laser ablation ICP-MS titanite U-Th-Pb dating of hydrothermal ore deposits A case study of the Tonglushan Cu-Fe-Au skarn deposit, SE Hubei Province. China. Chem. Geol. 270, 56–67.

Li, J.W., Vasconcelos, P.M., Zhou, M.F., Deng, X.D., Cohen, B., Bi, S.J., Zhao, X.F., Selby, D., 2014. Longevity of magmatic-hydrothermal systems in the Daye Cu-Fe-Au District, eastern China with implications for mineral exploration. Ore Geol. Rev. 57, 375–392.

Liu, Y.C., Yang, C.Y., Wang, Y.J., 2007. Investigation of ore controlling structures and prognosis of concealed ores in the Daye iron mine. Resour. Environ. Eng. 21, 10–16 (in Chinese with English abstract).

Liu, Y.S., Hu, Z.C., Gao, S., Gunther, D., Xu, J., Gao, C.G., Chen, H.H., 2008. In situ analysis of major and trace elements of anhydrous minerals by LA–ICP-MS without applying an internal standard. Chem. Geol. 257, 34–43.

Müller, B., Axelsson, M.D., Öhlander, B., 2003. Trace elements in magnetite from Kiruna, northern Sweden, as determined by LA-ICP-MS. GFF 125, 1–5.

Mao, J.W., Xie, G.Q., Duan, C., Pirajno, F., Ishiyama, D., Chen, Y.C., 2011. A tectono-genetic model for porphyry-skarn-stratabound Cu-Au-Mo-Fe and magnetite-apatite deposits along the Middle-Lower Yangtze River Valley, Eastern China. Ore Geol. Rev. 43, 294–314.

Nadoll, P., Koenig, A.E., 2011. LA-ICP-MS of magnetite: methods and reference materials. J. Anal. At. Spectrom. 26, 1872–1877.

Nadoll, P., Mauk, J.L., Hayes, T.S., Koenig, A.E., Box, S.E., 2012. Geochemistry of magnetite from hydrothermal ore deposits and host rocks of the Mesoproterozoic Belt Supergroup United States. Econ. Geol. 107, 1275–1292.

Nadoll, P., Angerer, T., Mauk, J.L., French, D., Walshe, J., 2014. The chemistry of hydrothermal magnetite: a review. Ore Geol. Rev. 61, 1–32.

Nadoll, P., Mauk, J., Leveille, R., Koenig, A., 2015. Geochemistry of magnetite from porphyry Cu and skarn deposits in the southwestern United States. Miner. Deposita 50, 493–515.

Nadoll, P., 2010. Geochemistry of Magnetite from Hydrothermal Ore Deposits and Host Rocks- Case Studies from the Proterozoic Belt Supergroup, Cu-Mo-porphyry+ Skam and Climax-Mo Deposits in the Western United States. The University of Auckland, Auckland.

Nesbitt, R.W., Hirata, T., Butler, I.B., Milton, J.A., 1997. UV laser ablation ICP-MS: Some applications in the earth sciences. Geostandards Newslett. 20, 231–243.

Nielsen, R.L., Forsythe, L.M., Gallahan, W.E., Fisk, M.R., 1994. Major-and trace-element magnetite-melt equilibria. Chem. Geol. 117, 167–191.

Pan, Y.M., Dong, P., 1999. The Lower Changjiang (Yangzi/Yangtze River) metallogenic belt, east central China: intrusion- and wall rock-hosted Cu-Fe-Au Mo, Zn, Pb, Ag deposits. Ore Geol. Rev. 15, 177–242.

Qu, H.Y., Wang, H.L., Pei, R.F., Yao, L., Wang, Y.L., Zheng, Z.G., 2012. Zircon U-Pb geochronological and Hf isotopic constraints on petrogenesis of Tieshan and Jinshandian plutons in the southeastern Hubei Province. Acta Petrologica Sin. 28, 147–165 (in Chinese with English abstract).

Reich, M., Simon, A.C., Deditius, A., Barra, F., Chryssoulis, S., Lagas, G., Tardani, D., Knipping, J., Bilenker, L., Sánchez-Alfaro, P., Roberts, M.P., Munizaga, R., 2016. Trace element signature of pyrite from the Los Colorados iron oxide-apatite (IOA) deposit, Chile: a missing link between Andean IOA and iron oxide copper-gold systems? Econ. Geol. 111, 743–761.

Rudnick, R.L., Gao, S., 2003. Composition of the continental crust. In: Holland, H.D., Turekian, K.K. (Eds.), Treatise on Geochemistry. Elsevier-Pergaman, Oxford, pp. 1–64.

Shi, Z.L., Jin, Z.M., Xiong, P.F., Wang, D.Y., Zhang, W.H., Chen, Z.Y., 1982. Geological Characteristics of the Daye Iron Deposit and Prognosis of Deep Mineral Resources. Wuhan College of Geology, Wuhan (in Chinese with English Abstract).

Shu, Q.A., Chen, P.L., Cheng, J.R., 1992. Geology of Iron–Copper Deposits in Eastern Hubei Province. Ministry of Metallurgical Industry Publishing House, Beijing, China (in Chinese with English Abstract).

Singoyi, B., Danyushevsky, L., Davidson, G., Large, R., Zaw, K., 2006. Determination of trace elements in magnetites from hydrothermal deposits using the LA ICP-MS technique. In: SEG Keystone Conference, Denver USA, pp. CD–ROM.

Toplis, M.J., Corgne, A., 2002. An experimental study of element partitioning between magnetite, clinopyroxene and iron-bearing silicate liquids with particular emphasis on vanadium. Contrib. Mineral. Petrol. 144, 22–37.

Wang, M.F., Guo, X.N., Chen, M.T., 2014a. Characteristics of composition of trace elements and PGE in magnetite. Contribut. Geol. Miner. Resources Res. 29, 417–423 (in Chinese with English abstract).

Wang, M.F., Gutzmer, J., Michalak, P.P., Guo, X.N., Xiao, F., Wang, W., Liu, K., 2014b. PGE geochemistry of the Fengshan porphyry-skarn Cu-Mo deposit, Hubei Province, Eastern China. Ore Geol. Rev. 56, 1–12.
Wang, S.J., 1987. Standard Features on the Type of Magnetite. China University of Geosciences Press, Wuhan (in Chinese with English abstract).
Whitney, D.L., Evans, B.W., 2010. Abbreviations for names of rock-forming minerals. Am. Mineral. 95, 185–187.
Xie, G.Q., Mao, J.W., Li, R.L., Bierlein, F.P., 2008. Geochemistry and Nd-Sr isotopic studies of Late Mesozoic granitoids in the southeastern Hubei Province, Middle-Lower Yangtze River belt, Eastern China: petrogenesis and tectonic setting. Lithos 104, 216–230.
Xie, G.Q., Mao, J.W., Zhao, H.J., Wei, K.T., Jin, S.G., Pan, H.J., Ke, Y.F., 2011. Timing of skarn deposit formation of the Tonglushan ore district, southeastern Hubei Province, Middle-Lower Yangtze River Valley metallogenic belt and its implications. Ore Geol. Rev. 43, 62–77.
Xie, G.Q., Mao, J.W., Zhu, Q.Q., Yao, L., Li, Y.H., Li, W., Zhao, H.J., 2015. Geochemical constraints on Cu-Fe and Fe skarn deposits in the Edong district, Middle-Lower Yangtze River metallogenic belt, China. Ore Geol. Rev. 64, 425–444.
Xie, G.Q., Mao, J.W., Li, W., Zhu, Q.Q., Liu, H.B., Jia, G.H., Li, Y.H., Li, J.J., Zhang, J., 2016. Different proportion of mantle-derived noble gases in the Cu–Fe and Fe skarn deposits: He–Ar isotopic constraint in the Edong district, Eastern China. Ore Geol. Rev. 72 (Part (1)), 343–354.
Xu, G.F., Shao, J.L., 1979. Typomorphic characteristics of magnetite and its practical significance. Geol. Explor. 3, 30–37 (in Chinese).
Zhai, Y.S., Yao, S.Z., Lin, X.D., Zhou, X.R., 1992. Metallogeny of Fe-Cu-(Au) ore deposits in Middle-Lower Changjiang. Miner. Deposits 11, 1–12 (in Chinese with English abstract).
Zhai, Y.S., Xiong, S.Z., Yao, Y., Lin, X.D., 1996. Metallogeny of copper and iron deposits in the Eastern Yangtse Craton east-central China. Ore Geol. Rev. 11, 229–248.
Zhao, W.W., Zhou, M.F., 2015. In-situ LA-ICP-MS trace elemental analyses of magnetite: the Mesozoic Tengtie skarn Fe deposit in the Nanling Range, South China. Ore Geol. Rev. 65, 872–883 (Part 4).
Zhao, A.X., 1990. A study on the mineral chemistry of magnetite from Tieshan iron-copper mineral deposit, Daye, Hubei and its origin. Earth Sci.-J. China Univ. Geosci. 15, 385–396 (in Chinese with English abstract).
Zhao, Y.X., 1993. Formation Mechanism of Contact-type Iron Ore Deposits in the Middle-Lower Yangtze River Valley. China University of Geosciences Press, Wuhan (in Chinese with English abstract).
Zhou, T.F., Wang, S.W., Fan, Y., Yuan, F., Zhang, D.Y., White, N.C., 2015. A review of the intracontinental porphyry deposits in the Middle-Lower Yangtze River Valley metallogenic belt Eastern China. Ore Geol. Rev. 65 (Part (1)), 433–456.